

Effect of vector meson spin coherence on the observables for the chiral magnetic effect in heavy-ion collisions

Zhiyi Wang,^{1,2} Jinhui Chen,^{1,2} Diyu Shen,^{1,2,*} Aihong Tang,³ and Gang Wang⁴

¹*Key Laboratory of Nuclear Physics and Ion-beam Application (MOE),
Institute of Modern Physics, Fudan University, Shanghai 200433, China*

²*Shanghai Research Center for Theoretical Nuclear Physics,
NSFC and Fudan University, Shanghai 200438, China*

³*Brookhaven National Laboratory, Upton, New York 11973, USA*

⁴*Department of Physics and Astronomy, University of California, Los Angeles, California 90095, USA*

(Dated: September 10, 2024)

The chiral magnetic effect (CME) in heavy-ion collisions reflects the local violation of \mathcal{P} and \mathcal{CP} symmetries in strong interactions and manifests as electric charge separation along the direction of the magnetic field created by the wounded nuclei. The experimental observables for the CME, such as the γ_{112} correlator, the $R_{\Psi_2}(\Delta S)$ correlator, and the signed balance functions, however, are also subject to non-CME backgrounds, including those from resonance decays. A previous study showed that the CME observables are affected by the diagonal component of the spin density matrix, the ρ_{00} for vector mesons. In this work, we study the contributions from the other elements of the spin density matrix using a toy model and a multiphase transport model. We find that the real part of the ρ_{1-1} component, $\text{Re } \rho_{1-1}$, affects the CME observables in a manner opposite to that of the ρ_{00} . All three aforementioned CME observables show a linear dependence on $\text{Re } \rho_{1-1}$ in the model calculations, supporting our analytical derivations. The rest elements of the spin density matrix do not contribute to the CME observables. The off-diagonal terms in the spin density matrix indicate spin coherence and may be nonzero in heavy-ion collisions due to local spin polarization or spin-spin correlations. Thus, $\text{Re } \rho_{1-1}$, along with ρ_{00} , could play a significant role in interpreting measurements in search of the CME.

I. INTRODUCTION

Experiments in heavy-ion collisions at Relativistic Heavy Ion Collider (RHIC) and the Large Hadron Collider (LHC) can create a deconfined nuclear matter known as quark-gluon plasma (QGP) [1–7], providing a unique test ground for quantum chromodynamics (QCD). Particularly, the chiral magnetic effect (CME) probes the topological vacuum transition in QCD [8, 9], whereby \mathcal{P} and \mathcal{CP} symmetries may be locally violated in strong interactions. The CME predicts electric charge separation along the magnetic field generated in heavy-ion collisions [10–12]. Several experimental observables have been proposed to detect the CME-induced charge separation, such as the γ_{112} correlator [13], the $R_{\Psi_2}(\Delta S)$ correlator [14], and signed balance functions [15], with their core components found to be equivalent [16]. The search for the CME using these observables has been extensively conducted at RHIC and the LHC over the past two decades [17–28]. However, a firm conclusion on the existence of the CME in such experiments remains elusive, as data interpretation is impeded by the incomplete understanding of non-CME backgrounds, especially those related to the collective motion or elliptic flow (v_2) of the collision system [29–34].

Besides the flow-related backgrounds, our prior study showed that the 00-component of the spin density matrix

for vector mesons, the ρ_{00} , could also affect the CME observables because of the anisotropic decay pattern of two oppositely charged daughters [35]. In such studies, the spin density matrix is defined along the direction perpendicular to the reaction plane (spanned by impact parameter and beam momenta),

$$\rho^V = \begin{pmatrix} \rho_{11} & \rho_{10} & \rho_{1-1} \\ \rho_{01} & \rho_{00} & \rho_{0-1} \\ \rho_{-11} & \rho_{-10} & \rho_{-1-1} \end{pmatrix}, \quad (1)$$

where the indices 1, 0, and -1 label the vector meson's spin components along the spin-quantization axis. The deviation of ρ_{00} from $1/3$ with respect to the reaction plane is known as the global spin alignment effect [36, 37], which has been measured in experiment for several vector mesons, such as ϕ , K^{*0} [38–40], and J/Ψ [41]. The observed global spin alignment effects for those mesons are unexpectedly large compared to predictions based on the global polarization of Λ hyperons [42–45], suggesting rich physics mechanisms beyond spin-orbital coupling, e.g., the strong electromagnetic fields [12, 46, 47], local spin alignment [48, 49], as well as novel phenomena such as fluctuation of strong vector meson fields [47, 50–54] and/or local axial charge currents [55]. All those mechanisms will cause ρ_{00} to deviate from $1/3$, resembling an apparent charge-separation. Therefore, the background contribution from ρ_{00} to the CME observables cannot be ignored.

The off-diagonal elements in the spin density matrix reflect the spin coherence between the states 1, 0, and -1 , and could be finite due to various physics effects.

* dyshen@fudan.edu.cn

For example, local spin alignment [48] can result in a nonzero real part of the ρ_{1-1} component, the $\text{Re } \rho_{1-1}$, in central collisions. Spin-spin correlations [56] could also lead to nonzero off-diagonal elements, depending on the difference in the correlation strength between different directions. Finite $\text{Re } \rho_{1-1}$ values have been observed in lepton-induced reactions and hadron-hadron collisions, such as those for K^{*0} in e^+e^- collisions at the Large Electron-Positron Collider (LEP) [57]. In this article, we adopt the framework from Ref. [35] and study the impact of all components of the spin density matrix on the CME observables through the decay of $\rho \rightarrow \pi^+\pi^-$. For each of the aforementioned CME observables, we first perform an analytical derivation and then use a toy model and a multiphase transport model (AMPT) [58] to confirm the findings.

II. THE γ_{112} CORRELATOR

The CME-induced electric dipole breaks the up-down symmetry across the reaction plane, resulting in nonzero sine terms in the azimuthal angle distribution of final-state particles [13],

$$\frac{dN_{\pm}}{d\varphi} \propto 1 + 2a_1^{\pm} \sin \Delta\varphi + \sum_{n=1}^{\infty} 2v_n^{\pm} \cos(n\Delta\varphi), \quad (2)$$

where $\Delta\varphi = \varphi - \Psi_{\text{RP}}$ is the azimuthal angle of a particle relative to the reaction plane (Ψ_{RP}). a_1^{\pm} characterizes the strength of charge separation with opposite signs for oppositely charged particles. v_n^{\pm} denotes the n^{th} -harmonic flow coefficient of final-state particles, with v_2 conventionally denoting the elliptic flow.

Since \mathcal{P} is only locally violated but globally conserved, the event average of a_1^{\pm} is zero. The CME has to be detected through fluctuations of charged particles. The γ_{112} correlator serves this purpose [13],

$$\gamma_{112} \equiv \langle \cos(\varphi_{\alpha} + \varphi_{\beta} - 2\Psi_{\text{RP}}) \rangle, \quad (3)$$

where φ_{α} and φ_{β} are the azimuthal angles of charged particles α and β , respectively. The bracket denotes averaging over all particle pairs and all events. The CME signal is contained in the difference between the opposite-sign (OS) and same-sign (SS) pairs,

$$\Delta\gamma_{112} \equiv \gamma_{112}^{\text{OS}} - \gamma_{112}^{\text{SS}} \approx 2|a_1^{\pm}|^2. \quad (4)$$

However, $\Delta\gamma_{112}$ is contaminated with charge-dependent backgrounds, while charge-independent ones are canceled out. We express the contribution from the decay of $\rho \rightarrow \pi^+ + \pi^-$ as described in Ref. [35],

$$\Delta\gamma_{112}^{\rho} = \frac{N_{\rho}}{N_+N_-} \left[\text{Cov}(\cos \Delta\varphi_+, \cos \Delta\varphi_-) - \text{Cov}(\sin \Delta\varphi_+, \sin \Delta\varphi_-) \right], \quad (5)$$

where $\text{Cov}(a, b)$ denotes the covariance of variables a and b . N_{ρ} is the yield of ρ meson, and N_+ and N_- are the numbers of π^+ and π^- , respectively.

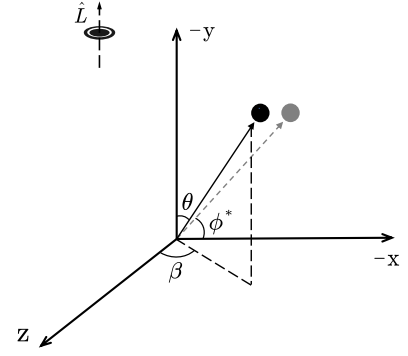


FIG. 1. Sketch of pion emission (solid arrow) in the rest frame of the parent ρ meson. The impact parameter and the beam direction are aligned along the x and z axes, respectively. The dashed arrow represents the projection in the x - y plane.

Figure 1 illustrates pion emission in the rest frame of the parent ρ meson, where θ is the angle between the pion momentum (\vec{p}) and the system total angular momentum \hat{L} , ϕ^* is the azimuthal angle, and β is the angle between the z axis and the projection of \vec{p} onto the x - z plane. Incorporating all elements of the spin density matrix, we write the distribution of the π^{\pm} emission angle as outlined in Ref. [48],

$$\begin{aligned} \frac{d^2N}{d(\cos\theta)d\beta} = & \frac{3}{8\pi} \left[(1 - \rho_{00}) + (3\rho_{00} - 1) \cos^2\theta \right. \\ & - \sqrt{2}\text{Re}(\rho_{10} - \rho_{0-1}) \sin(2\theta) \cos\beta \\ & + \sqrt{2}\text{Im}(\rho_{10} - \rho_{0-1}) \sin(2\theta) \sin\beta \\ & - 2\text{Re} \rho_{1-1} \sin^2\theta \cos(2\beta) \\ & \left. + 2\text{Im} \rho_{1-1} \sin^2\theta \sin(2\beta) \right]. \quad (6) \end{aligned}$$

The projection of Eq. (6) to the transverse plane (x - y) becomes

$$\begin{aligned} \frac{dN}{d\phi^*} = & \frac{1}{2\pi} \left[1 - \frac{1}{2}(3\rho_{00} - 1) \cos 2\phi^* \right. \\ & \left. + \sqrt{2}\text{Im}(\rho_{10} - \rho_{0-1}) \sin 2\phi^* + \text{Re} \rho_{1-1} \cos 2\phi^* \right]. \quad (7) \end{aligned}$$

Then, the covariance terms in Eq. (5) can be calculated in the rest frame of the ρ meson as

$$\begin{aligned} \text{Cov}(\cos \phi_+^*, \cos \phi_-^*) = & -\langle \cos^2 \phi_+^* \rangle + \langle \cos \phi_+^* \rangle^2 \\ = & -\frac{1}{2} + \frac{3\rho_{00} - 1}{8} - \frac{\text{Re} \rho_{1-1}}{4}, \quad (8) \end{aligned}$$

$$\begin{aligned} \text{Cov}(\sin \phi_+^*, \sin \phi_-^*) = & -\langle \sin^2 \phi_+^* \rangle + \langle \sin \phi_+^* \rangle^2 \\ = & -\frac{1}{2} - \frac{3\rho_{00} - 1}{8} + \frac{\text{Re} \rho_{1-1}}{4}. \quad (9) \end{aligned}$$

Here we take $\phi_-^* = \phi_+^* + \pi$. Therefore, the decay contribution $\Delta\gamma_{112}^{\rho}$ in Eq. (5) becomes

$$\Delta\gamma_{112}^{\rho*} = \frac{N_{\rho}}{N_+N_-} \left[\frac{3}{4}(\rho_{00} - \frac{1}{3}) - \frac{1}{2}\text{Re} \rho_{1-1} \right], \quad (10)$$

in the ρ rest frame. Apparently, both ρ_{00} and $\text{Re}\rho_{1-1}$ could contribute to the $\Delta\gamma_{112}$ correlator, whereas all other elements of the spin density matrix can be safely ignored.

Back in the laboratory frame, Eqs. (8) and (9) need to be scaled by factors of f_c and f_s , respectively, due to the Lorentz boost of the ρ meson [35]. In general, f_c and f_s are different because of the anisotropic collective motion (v_2^{ρ}) of ρ mesons. Since the elliptic flow effect has been discussed previously [35], we assume v_2^{ρ} is zero for simplicity. Hence, the background contribution of decay pions to $\Delta\gamma_{112}$ in the laboratory frame can be expressed as

$$\Delta\gamma_{112}^{\rho} = f_0 \frac{N_{\rho}}{N_{+}N_{-}} \left[\frac{3}{4}(\rho_{00} - \frac{1}{3}) - \frac{1}{2}\text{Re}\rho_{1-1} \right], \quad (11)$$

where the coefficient f_0 absorbs the Lorentz boost effects and should depend on the spectrum of the ρ meson [35].

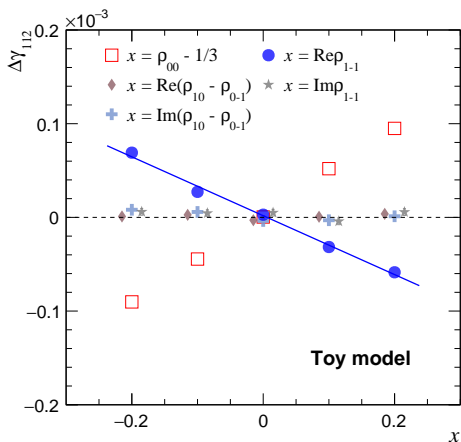


FIG. 2. Toy model simulations of the π - π $\Delta\gamma_{112}$ correlation vs various elements of the ρ -meson spin density matrix: $\rho_{00}-1/3$, $\text{Re}(\rho_{10} - \rho_{0-1})$, $\text{Im}(\rho_{10} - \rho_{0-1})$, $\text{Re}\rho_{1-1}$, and $\text{Im}\rho_{1-1}$. v_2^{ρ} is set to zero. The solid line represents the linear fit to the case $x = \text{Re}\rho_{1-1}$.

We first test the analytical derivation using toy model simulations without the CME. We follow the same implementations as in the previous study [35], updating the momentum distribution of ρ -meson decay products according to Eq. (6). We set v_2^{ρ} to be zero. Figure 2 shows the simulation results of the π - π $\Delta\gamma_{112}$ correlation as a function of $\rho_{00} - 1/3$, $\text{Re}(\rho_{10} - \rho_{0-1})$, $\text{Im}(\rho_{10} - \rho_{0-1})$, $\text{Re}\rho_{1-1}$, and $\text{Im}\rho_{1-1}$, respectively. $\Delta\gamma_{112}$ is linearly correlated with ρ_{00} but anti-correlated with $\text{Re}\rho_{1-1}$, supporting Eq. (11), where ρ_{00} and $\text{Re}\rho_{1-1}$ have comparable but opposite impacts on $\Delta\gamma_{112}$. Other components have no contributions to $\Delta\gamma_{112}$.

We also study this effect using AMPT simulations of Au+Au collisions at $\sqrt{s_{NN}} = 200$ GeV with an impact parameter of 8 fm. The details of this model can be found in Ref. [58]. The string-melting version of the AMPT

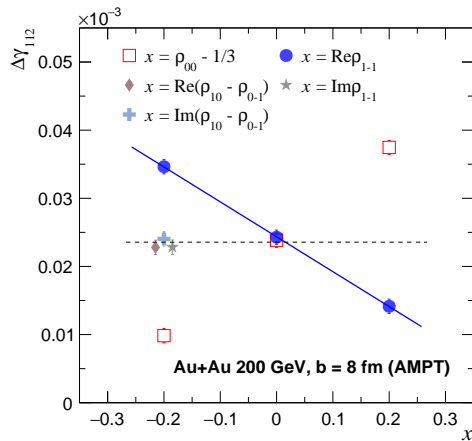


FIG. 3. AMPT calculations of the π - π $\Delta\gamma_{112}$ correlation vs various elements of the ρ -meson spin density matrix: $\rho_{00} - 1/3$, $\text{Re}(\rho_{10} - \rho_{0-1})$, $\text{Im}(\rho_{10} - \rho_{0-1})$, $\text{Re}\rho_{1-1}$, and $\text{Im}\rho_{1-1}$ in Au+Au collisions at $\sqrt{s_{NN}} = 200$ GeV with an impact parameter of 8 fm. The solid line denotes the linear fit for the case $x = \text{Re}\rho_{1-1}$, while the dashed line represents a constant to guide the eye for cases involving non-contributing elements.

model is used without the CME, and the selected decay channel is $\rho \rightarrow \pi^+ + \pi^-$. Pions are analyzed without any kinematic cut to increase statistics. The spin density matrix is implemented by redistributing the momenta of decay products according to Eq. (6), similar to the procedures in Refs. [59, 60]. The $\rho_{00} - 1/3$ and $\text{Re}\rho_{1-1}$ values are each set to be -0.2 , 0 , and 0.2 to test the linear dependence. The other elements are set to -0.2 solely to demonstrate their contribution or lack thereof. For each case, we have generated 2 million events. Figure 3 shows the linear correlation (anti-correlation) between $\Delta\gamma_{112}$ and ρ_{00} ($\text{Re}\rho_{1-1}$), akin to the toy model simulations. For other spin density matrix components, the $\Delta\gamma_{112}$ values at $x = -0.2$ are consistent with that at $x = 0$ within uncertainties, as demonstrated by a constant dashed line. The nonzero $\Delta\gamma_{112}$ value at $x = 0$ comes from the positive v_2^{ρ} and local charge conservation [30, 31]. Quantitatively, the slopes $d\Delta\gamma_{112}/d\rho_{00}$ and $d\Delta\gamma_{112}/d\text{Re}\rho_{1-1}$ depend on the ρ -meson spectrum.

III. THE $R_{\Psi_2}(\Delta S)$ CORRELATOR

Another CME observable, the $R_{\Psi_2}(\Delta S)$ correlator, focuses on the event-by-event fluctuations of a_1 and is defined as a double ratio of four distributions,

$$R_{\Psi_2}(\Delta S) \equiv \frac{N(\Delta S_{\text{real}})}{N(\Delta S_{\text{shuffled}})} / \frac{N(\Delta S_{\text{real}}^{\perp})}{N(\Delta S_{\text{shuffled}}^{\perp})}, \quad (12)$$

where

$$\Delta S = \langle \sin(\phi^+ - \Psi_2) \rangle - \langle \sin(\phi^- - \Psi_2) \rangle, \quad (13)$$

$$\Delta S^{\perp} = \langle \cos(\phi^+ - \Psi_2) \rangle - \langle \cos(\phi^- - \Psi_2) \rangle, \quad (14)$$

where ϕ^+ and ϕ^- are the azimuthal angles of positively and negatively charged particles, respectively. Ψ_2 represents the 2nd-order event plane, which serves as a proxy of the reaction plane and is estimated from the final-state hadron emission. The bracket denotes averaging over all particles in an event. The subscript ‘‘real’’ refers to using the actual charge information, while ‘‘shuffled’’ indicates reshuffling charges within the same event. Ideally, the CME-driven charge separation should cause a concave shape in $R_{\Psi_2}(\Delta S)$. By construction, the resulting concave or convex shape relies on the relative widths of the four individual $N(\Delta S)$ distributions. Therefore, as in our previous work [35], we introduce a straightforward variable to quantify the signal or background strength based on the four variances,

$$\Delta\sigma_R^2 = \sigma^2(\Delta S_{\text{real}}) - \sigma^2(\Delta S_{\text{shuffled}}) - \sigma^2(\Delta S_{\text{real}}^\perp) + \sigma^2(\Delta S_{\text{shuffled}}^\perp). \quad (15)$$

The CME signal corresponds to a positive $\Delta\sigma_R^2$.

Again, we set v_2^p to zero so that the Lorentz boost factor f_0 only depends on the ρ spectrum. Then, each term of Eq. (15) in the laboratory frame can be expressed as

$$\sigma^2(\Delta S_{\text{real}}) = f_0 \left[\sigma_s^2 - \frac{2N_\rho}{N_+N_-} \text{Cov}(\sin \Delta\phi_+, \sin \Delta\phi_-) \right], \quad (16)$$

$$\sigma^2(\Delta S_{\text{real}}^\perp) = f_0 \left[\sigma_c^2 - \frac{2N_\rho}{N_+N_-} \text{Cov}(\cos \Delta\phi_+, \cos \Delta\phi_-) \right], \quad (17)$$

$$\sigma^2(\Delta S_{\text{shuffled}}) = f_0 \sigma_s^2, \quad (18)$$

$$\sigma^2(\Delta S_{\text{shuffled}}^\perp) = f_0 \sigma_c^2, \quad (19)$$

where

$$\sigma_s^2 = \frac{\sigma^2(\sin \phi_+^*)}{N_+} + \frac{\sigma^2(\sin \phi_-^*)}{N_-}, \quad (20)$$

$$\sigma_c^2 = \frac{\sigma^2(\cos \phi_+^*)}{N_+} + \frac{\sigma^2(\cos \phi_-^*)}{N_-}. \quad (21)$$

The shared terms will be canceled out, leaving only the covariance terms in $\Delta\sigma_R^2$. According to Eqs. (8) and (9), the contribution of ρ -decay pions to $\Delta\sigma_R^2$ can be calculated as

$$\Delta\sigma_R^2 = f_0 \frac{N_\rho}{N_+N_-} \left[\frac{3}{2}(\rho_{00} - \frac{1}{3}) - \text{Re} \rho_{1-1} \right]. \quad (22)$$

Eq. (22) has a function form similar to that of Eq. (11), with $\Delta\sigma_R^2$ also exhibiting a linear dependence on ρ_{00} and $\text{Re} \rho_{1-1}$.

Alternatively, the CME signal can also be reflected in the difference between the inverse Gaussian widths,

$$\frac{S_{\text{concavity}}}{\sigma_R^2} = \frac{1}{\sigma^2(\Delta S_{\text{real}})} - \frac{1}{\sigma^2(\Delta S_{\text{shuffled}})} - \frac{1}{\sigma^2(\Delta S_{\text{real}}^\perp)} + \frac{1}{\sigma^2(\Delta S_{\text{shuffled}}^\perp)}. \quad (23)$$

$S_{\text{concavity}}$ is 1 (−1) when the $R_{\Psi_2}(\Delta S)$ distribution is convex (concave). After applying Eqs. (16, 17, 18, 19), we have

$$S_{\text{concavity}} = \text{Sign} \left[\text{Re} \rho_{1-1} - \frac{3}{2}(\rho_{00} - \frac{1}{3}) \right]. \quad (24)$$

At $\rho_{00} = 1/3$, a negative (positive) $\text{Re} \rho_{1-1}$ value corresponds to $S_{\text{concavity}} = -1$ (1) and a concave (convex) $R_{\Psi_2}(\Delta S)$ distribution.

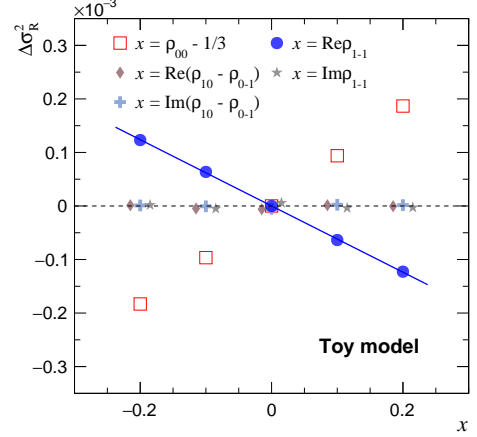


FIG. 4. Toy model simulations of $\Delta\sigma_R^2$ vs various elements of the ρ -meson spin density matrix: $\rho_{00} - 1/3$, $\text{Re}(\rho_{10} - \rho_{0-1})$, $\text{Im}(\rho_{10} - \rho_{0-1})$, $\text{Re} \rho_{1-1}$, and $\text{Im} \rho_{1-1}$. v_2^p is set to zero. The solid line represents the linear fit to the case $x = \text{Re} \rho_{1-1}$.

Figure 4 shows the toy-model simulations results of $\Delta\sigma_R^2$ as a function of each element of the ρ -meson spin density matrix, with the same settings as those for the $\Delta\gamma_{112}$ calculations. As expected, $\Delta\sigma_R^2$ exhibits a linear dependence on ρ_{00} and $\text{Re} \rho_{1-1}$, similar to the behavior of $\Delta\gamma_{112}$ in Fig. 2. This indicates that, in addition to global spin alignment, the off-diagonal elements resulting from spin coherence also influence the $R_{\Psi_2}(\Delta S)$ correlator. The other elements do not contribute to the $\Delta\sigma_R^2$.

To check the shape of the $R_{\Psi_2}(\Delta S)$ distribution, we adopt the same procedure as described in Ref. [14] to correct for the effect of multiplicity fluctuations, by defining $\Delta S'' = \Delta S/\sigma_{\text{sh}}$. Here, σ_{sh} represents the width of $N(\Delta S_{\text{shuffled}})$. Figure 5 (left) shows the $R_{\Psi_2}(\Delta S'')$ distributions with several $\text{Re} \rho_{1-1}$ values from the toy model simulations, where v_2^p and ρ_{00} are set to 0 and 1/3, respectively. $\text{Re} \rho_{1-1}$ varies from −0.2 to 0.2. When $\text{Re} \rho_{1-1}$ is positive (negative), the $R_{\Psi_2}(\Delta S'')$ distribution exhibits a convex (concave) shape. Moreover, a larger magnitude of $\text{Re} \rho_{1-1}$ corresponds to a narrower $R_{\Psi_2}(\Delta S'')$ distribution. Figure 5 (right) shows the $S_{\text{concavity}}/\sigma_R^2$ values extracted using Eq. (23) for different $\text{Re} \rho_{1-1}$ inputs, with a clear rising trend. $S_{\text{concavity}}$ appears to bear the same sign as $\text{Re} \rho_{1-1}$, which supports the analytical derivation.

Figure 6 shows the AMPT calculations of the $R_{\Psi_2}(\Delta S'')$ distribution with $\text{Re} \rho_{1-1} = -0.2, 0$, and

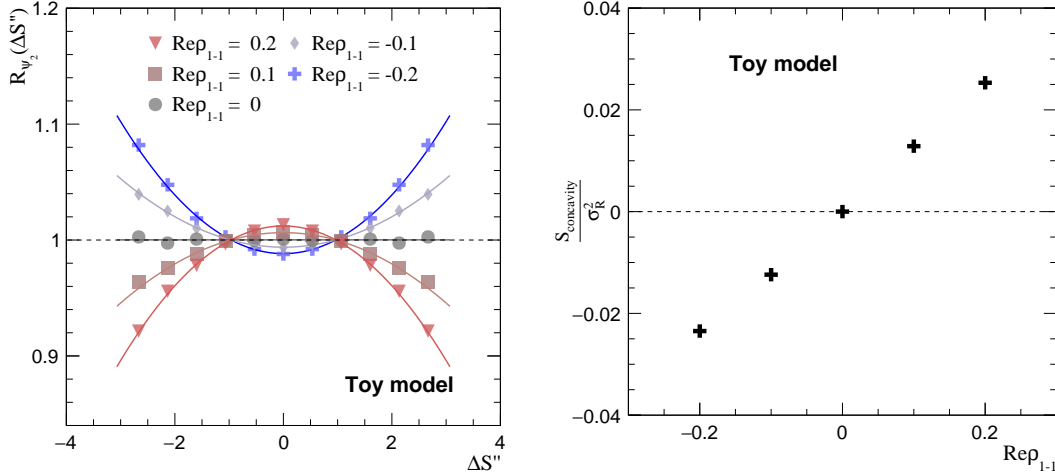


FIG. 5. (Left) toy model simulations of the $R_{\Psi_2}(\Delta S'')$ distribution with several $\text{Re } \rho_{1-1}$ inputs. v_2^p and ρ_{00} are set to 0 and $1/3$, respectively. The distributions are symmetrized around $\Delta S'' = 0$. (Right) The $S_{\text{concavity}}/\sigma_R^2$ values extracted using Gaussian fits to the $R_{\Psi_2}(\Delta S'')$ distributions at different $\text{Re } \rho_{1-1}$.

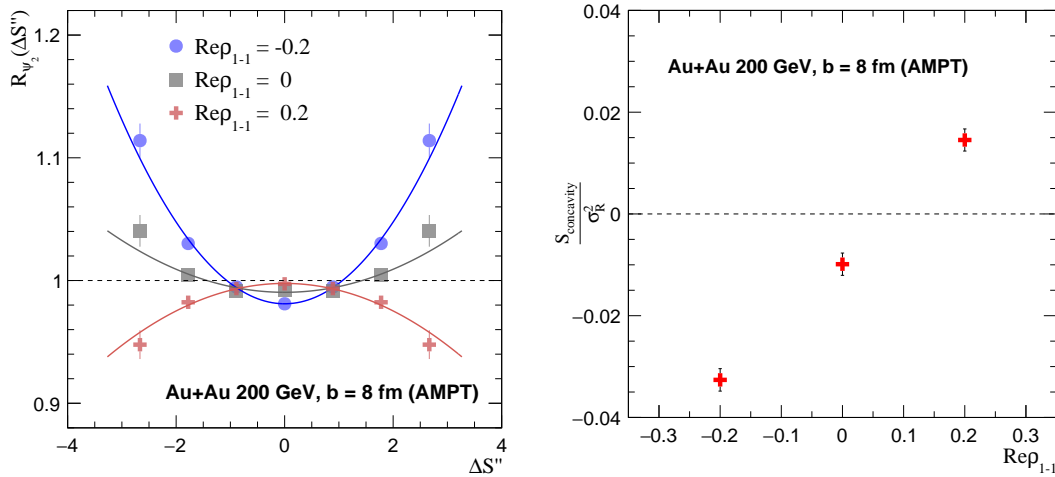


FIG. 6. (Left) AMPT calculations of the $R_{\Psi_2}(\Delta S'')$ distribution with $\text{Re } \rho_{1-1} = 0.2, 0,$ and -0.2 in Au+Au collisions at $\sqrt{s_{NN}} = 200$ GeV with an impact parameter of 8 fm. ρ_{00} is set to $1/3$. The distributions are symmetrized around $\Delta S'' = 0$. (Right) $S_{\text{concavity}}/\sigma_R^2$ extracted using Gaussian fits vs $\text{Re } \rho_{1-1}$.

0.2 in Au+Au collisions at $\sqrt{s_{NN}} = 200$ GeV with an impact parameter of 8 fm. ρ_{00} is set to $1/3$. In contrast to the toy-model results, the $R_{\Psi_2}(\Delta S'')$ distribution manifests a concave shape at zero $\text{Re } \rho_{1-1}$, which suggests a non-CME background due to the positive v_2^p value and the local charge conservation effect. Figure 6 (right) presents the $S_{\text{concavity}}/\sigma_R^2$ values retrieved using Gaussian fits, showing a linear dependence on $\text{Re } \rho_{1-1}$, similar to the toy-model outcomes. Thus, the AMPT calculations further confirm the background contribution of ρ -meson spin coherence to the $R_{\Psi_2}(\Delta S)$ correlator. Note that a quantitative estimation depends on model details, as evidenced by the difference between the toy model and

the AMPT.

IV. SIGNED BALANCE FUNCTIONS

Signed balance functions probe the CME by examining the momentum ordering between two charged particles,

based on the following quantity [15, 16]

$$\begin{aligned}\Delta B_y &\equiv \frac{N_{y(+)} - N_{y(++)}}{N_+} - \frac{N_{y(-)} - N_{y(--)}}{N_-} \\ &\quad - \frac{N_{y(-)} - N_{y(++)}}{N_+} + \frac{N_{y(+)} - N_{y(--)}}{N_-} \\ &= \frac{N_+ + N_-}{N_+ N_-} [N_{y(+)} - N_{y(-)}],\end{aligned}\quad (25)$$

where $N_{y(\alpha\beta)}$ is the number of pairs in which particle α is ahead of particle β along the y axis ($p_y^\alpha > p_y^\beta$) in an event. Similarly, ΔB_x can be constructed as a reference along the x axis,

$$\Delta B_x = \frac{N_+ + N_-}{N_+ N_-} [N_{x(+)} - N_{x(-)}].\quad (26)$$

The CME-induced charge separation along the y axis enhances the width of the ΔB_y distribution, but not that of the ΔB_x distribution. Therefore, the final observable is the ratio

$$r \equiv \sigma(\Delta B_y)/\sigma(\Delta B_x).\quad (27)$$

r can be calculated in either the laboratory frame (r_{lab}) or the pair's rest frame (r_{rest}). Since the extra sensitivity in r_{rest} is a higher-order effect requiring substantially more statistics and computing resources, we only focus on r_{lab} in this work. As suggested in Refs. [16, 35], we use a more straightforward definition based on the difference instead of the ratio to simplify the analytical derivation,

$$\Delta\sigma^2(\Delta B) \equiv \sigma^2(\Delta B_y) - \sigma^2(\Delta B_x),\quad (28)$$

where (see the appendix of Ref. [35] for details)

$$\sigma^2(\Delta B_y) \approx \frac{64M^2}{\pi^4} \left(\frac{4}{9M} + 1 \right) \sigma^2(\Delta S_{\text{real}}),\quad (29)$$

$$\sigma^2(\Delta B_x) \approx \frac{64M^2}{\pi^4} \left(\frac{4}{9M} + 1 \right) \sigma^2(\Delta S_{\text{real}}^\perp).\quad (30)$$

Here, M is the total multiplicity of all charged particles. According to Eqs. (16) and (17), we can relate $\sigma(\Delta B_y)$ and $\sigma(\Delta B_x)$ to the key components of the $R_{\Psi_2}(\Delta S)$ correlator, and thus rewrite $\Delta\sigma^2(\Delta B)$ as

$$\Delta\sigma^2(\Delta B) \approx c_1 + c_2 \left[\frac{3}{2}(\rho_{00} - \frac{1}{3}) - \text{Re} \rho_{1-1} \right],\quad (31)$$

where c_1 and c_2 are constant coefficients that depend on the ρ -meson spectrum, v_2^ρ , and v_2^π .

Figure 7 shows the toy model simulations of $\Delta\sigma^2(\Delta B)$ as a function of each element of the ρ -meson spin density matrix, with the same settings as those for the $\Delta\gamma_{112}$ calculations. Among the off-diagonal elements, only $\text{Re} \rho_{1-1}$ has nonzero contributions to $\Delta\sigma^2(\Delta B)$, exerting an effect opposite to that of ρ_{00} . The function forms of Eqs. (11), (22), and (31) are very similar to each other, as manifested in Figs. 2, 4, and 7. Therefore, this further consolidates that these observables have the same sensitivity to backgrounds.

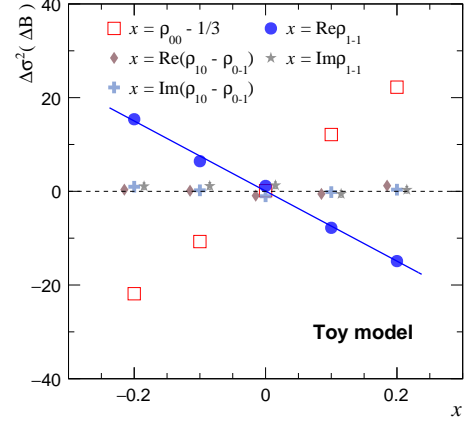


FIG. 7. Toy model simulations of $\Delta\sigma^2(\Delta B)$ vs various elements of the ρ -meson spin density matrix: $\rho_{00} - 1/3$, $\text{Re}(\rho_{10} - \rho_{0-1})$, $\text{Im}(\rho_{10} - \rho_{0-1})$, $\text{Re} \rho_{1-1}$, and $\text{Im} \rho_{1-1}$. v_2^ρ is set to zero. The solid line represents the linear fit to the case $x = \text{Re} \rho_{1-1}$.

Figure 8 shows the AMPT calculations of $\Delta\sigma^2(\Delta B)$ in Au+Au collisions at $\sqrt{s_{NN}} = 200$ GeV with an impact parameter of 8 fm, adopting the same input values of the spin density matrix elements as in Fig. 3. The linear dependence of $\Delta\sigma^2(\Delta B)$ on ρ_{00} and $\text{Re} \rho_{1-1}$ is akin to the toy model simulations. The positive $\Delta\sigma^2(\Delta B)$ at $x = 0$ may originate from the positive v_2^ρ and the local charge conservation effect. Quantitatively, the slopes $d\Delta\sigma^2(\Delta B)/d\rho_{00}$ and $d\Delta\sigma^2(\Delta B)/d\text{Re} \rho_{1-1}$ rely on the specific ρ -meson spectrum.

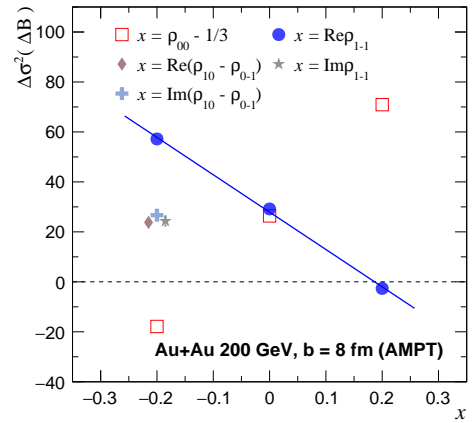


FIG. 8. AMPT calculations of $\Delta\sigma^2(\Delta B)$ vs various elements of the ρ -meson spin density matrix: $\rho_{00} - 1/3$, $\text{Re}(\rho_{10} - \rho_{0-1})$, $\text{Im}(\rho_{10} - \rho_{0-1})$, $\text{Re} \rho_{1-1}$, and $\text{Im} \rho_{1-1}$ in Au+Au collisions at $\sqrt{s_{NN}} = 200$ GeV with an impact parameter of 8 fm. The solid line denotes the linear fit for the case $x = \text{Re} \rho_{1-1}$.

V. SUMMARY

The chiral magnetic effect in high-energy heavy-ion collisions addresses a fundamental question in modern physics: whether parity can be violated in strong interactions. However, the experimental search for the CME has not reached a definitive conclusion because of the complications stemming from the non-CME backgrounds in the observables. In this work, we extend our previous study [35] and demonstrate that not only the global spin alignment (ρ_{00}) of vector mesons but also the real part of the off-diagonal element, the $\text{Re } \rho_{1-1}$, can have a non-negligible contribution to the major CME observables.

For each of the $\Delta\gamma_{112}$ correlator, the $R_{\Psi_2}(\Delta S)$ correlator, and the signed balance functions, we analytically derive its qualitative dependence on the elements of the vector meson spin density matrix and find that only ρ_{00} and $\text{Re } \rho_{1-1}$ could yield finite contributions. The effect of $\text{Re } \rho_{1-1}$ is comparable in magnitude to that of ρ_{00} but acts in the opposite direction. We use the ρ -meson decays from a toy model and the AMPT model to verify the linear dependence of each CME observable on $\text{Re } \rho_{1-1}$. This further confirms the equivalent sensitivity of these three observables to both the CME signal and backgrounds.

The nonzero off-diagonal components in the spin density matrix, known as spin coherence, could have non-CME origins, such as local spin alignment [48] and short-

range spin-spin correlations [56]. Hence, the $\text{Re } \rho_{1-1}$ of vector mesons represents a physics background to CME observables involving the decay products. On the other hand, Eqs. (11), (22), and (31) are not necessarily unidirectional. As noted in Ref. [61], global spin alignment may also arise from the CME. For instance, the CME induces charge separation of π^+ and π^- , some of which later coalesce into ρ mesons with $\rho_{00} \neq 1/3$. Similarly, we cannot rule out the possibility that a finite $\text{Re } \rho_{1-1}$ stems from the CME. The interaction between the CME and the elements of the spin density matrix warrants further theoretical investigation.

ACKNOWLEDGEMENT

Zhiyi Wang and Jinhui Chen are supported, in part, by the National Key Research and Development Program of China under Contract No. 2022YFA1604900, by the National Natural Science Foundation of China (NSFC) under Contract No. 12025501 and the Natural Science Foundation of Shanghai under Contract No. 23JC1400200. Diyu Shen is supported by the NSFC under Contract No. 12205050. Gang Wang is supported by the U.S. Department of Energy under Grant No. DE-FG02-88ER40424 and by the NSFC under Contract No. 1835002. Aihong Tang is supported by the US Department of Energy under Grants No. DE-AC02-98CH10886, DE-FG02-89ER40531.

-
- [1] E. V. Shuryak, Quantum Chromodynamics and the Theory of Superdense Matter, *Phys. Rept.* 61 (1980) 71–158. doi:doi:10.1016/0370-1573(80)90105-2.
 - [2] I. Arsene, et al. (BRAHMS), Quark gluon plasma and color glass condensate at RHIC? The Perspective from the BRAHMS experiment, *Nucl. Phys. A* 757 (2005) 1–27. doi:doi:10.1016/j.nuclphysa.2005.02.130. [arXiv:nucl-ex/0410020](#).
 - [3] B. B. Back, et al. (PHOBOS), The PHOBOS perspective on discoveries at RHIC, *Nucl. Phys. A* 757 (2005) 28–101. doi:doi:10.1016/j.nuclphysa.2005.03.084. [arXiv:nucl-ex/0410022](#).
 - [4] J. Adams, et al. (STAR), Experimental and theoretical challenges in the search for the quark gluon plasma: The STAR Collaboration’s critical assessment of the evidence from RHIC collisions, *Nucl. Phys. A* 757 (2005) 102–183. doi:doi:10.1016/j.nuclphysa.2005.03.085. [arXiv:nucl-ex/0501009](#).
 - [5] K. Adcox, et al. (PHENIX), Formation of dense partonic matter in relativistic nucleus-nucleus collisions at RHIC: Experimental evaluation by the PHENIX collaboration, *Nucl. Phys. A* 757 (2005) 184–283. doi:doi:10.1016/j.nuclphysa.2005.03.086. [arXiv:nucl-ex/0410003](#).
 - [6] W. Busza, K. Rajagopal, W. van der Schee, Heavy Ion Collisions: The Big Picture, and the Big Questions, *Ann. Rev. Nucl. Part. Sci.* 68 (2018) 339–376. doi:doi:10.1146/annurev-nucl-101917-020852. [arXiv:1802.04801](#).
 - [7] J. Chen, D. Keane, Y.-G. Ma, A. Tang, Z. Xu, Antinuclei in Heavy-Ion Collisions, *Phys. Rept.* 760 (2018) 1–39. doi:doi:10.1016/j.physrep.2018.07.002. [arXiv:1808.09619](#).
 - [8] D. E. Kharzeev, L. D. McLerran, H. J. Warringa, The Effects of topological charge change in heavy ion collisions: ‘Event by event P and CP violation’, *Nucl. Phys. A* 803 (2008) 227–253. doi:doi:10.1016/j.nuclphysa.2008.02.298. [arXiv:0711.0950](#).
 - [9] K. Fukushima, D. E. Kharzeev, H. J. Warringa, The Chiral Magnetic Effect, *Phys. Rev. D* 78 (2008) 074033. doi:doi:10.1103/PhysRevD.78.074033. [arXiv:0808.3382](#).
 - [10] V. Voronyuk, V. D. Toneev, W. Cassing, E. L. Bratkovskaya, V. P. Konchakovski, S. A. Voloshin, (Electro-)Magnetic field evolution in relativistic heavy-ion collisions, *Phys. Rev. C* 83 (2011) 054911. doi:doi:10.1103/PhysRevC.83.054911. [arXiv:1103.4239](#).
 - [11] W.-T. Deng, X.-G. Huang, Event-by-event generation of electromagnetic fields in heavy-ion collisions, *Phys. Rev. C* 85 (2012) 044907. doi:doi:10.1103/PhysRevC.85.044907. [arXiv:1201.5108](#).
 - [12] M. I. Abdulhamid, et al. (STAR), Observation of the electromagnetic field effect via charge-dependent directed flow in heavy-ion collisions at the Relativistic Heavy Ion Collider, *Phys. Rev. X* 14 (2024) 011028. doi:doi:10.1103/PhysRevX.14.011028. [arXiv:2304.03430](#).

- [13] S. A. Voloshin, Parity violation in hot QCD: How to detect it, *Phys. Rev. C* 70 (2004) 057901. doi:doi:10.1103/PhysRevC.70.057901. [arXiv:hep-ph/0406311](#).
- [14] N. Magdy, S. Shi, J. Liao, N. Ajitanand, R. A. Lacey, New correlator to detect and characterize the chiral magnetic effect, *Phys. Rev. C* 97 (2018) 061901. doi:doi:10.1103/PhysRevC.97.061901. [arXiv:1710.01717](#).
- [15] A. H. Tang, Probe chiral magnetic effect with signed balance function, *Chin. Phys. C* 44 (2020) 054101. doi:doi:10.1088/1674-1137/44/5/054101. [arXiv:1903.04622](#).
- [16] S. Choudhury, et al., Investigation of experimental observables in search of the chiral magnetic effect in heavy-ion collisions in the STAR experiment *, *Chin. Phys. C* 46 (2022) 014101. doi:doi:10.1088/1674-1137/ac2a1f. [arXiv:2105.06044](#).
- [17] B. I. Abelev, et al. (STAR), Azimuthal Charged-Particle Correlations and Possible Local Strong Parity Violation, *Phys. Rev. Lett.* 103 (2009) 251601. doi:doi:10.1103/PhysRevLett.103.251601. [arXiv:0909.1739](#).
- [18] L. Adamczyk, et al. (STAR), Fluctuations of charge separation perpendicular to the event plane and local parity violation in $\sqrt{s_{NN}} = 200$ GeV Au+Au collisions at the BNL Relativistic Heavy Ion Collider, *Phys. Rev. C* 88 (2013) 064911. doi:doi:10.1103/PhysRevC.88.064911. [arXiv:1302.3802](#).
- [19] L. Adamczyk, et al. (STAR), Beam-energy dependence of charge separation along the magnetic field in Au+Au collisions at RHIC, *Phys. Rev. Lett.* 113 (2014) 052302. doi:doi:10.1103/PhysRevLett.113.052302. [arXiv:1404.1433](#).
- [20] M. Abdallah, et al. (STAR), Search for the chiral magnetic effect with isobar collisions at $\sqrt{s_{NN}}=200$ GeV by the STAR Collaboration at the BNL Relativistic Heavy Ion Collider, *Phys. Rev. C* 105 (2022) 014901. doi:doi:10.1103/PhysRevC.105.014901. [arXiv:2109.00131](#).
- [21] B. Aboona, et al. (STAR), Search for the Chiral Magnetic Effect in Au+Au collisions at $\sqrt{s_{NN}} = 27$ GeV with the STAR forward Event Plane Detectors, *Phys. Lett. B* 839 (2023) 137779. doi:doi:10.1016/j.physletb.2023.137779. [arXiv:2209.03467](#).
- [22] B. Abelev, et al. (ALICE), Charge separation relative to the reaction plane in Pb-Pb collisions at $\sqrt{s_{NN}} = 2.76$ TeV, *Phys. Rev. Lett.* 110 (2013) 012301. doi:doi:10.1103/PhysRevLett.110.012301. [arXiv:1207.0900](#).
- [23] V. Khachatryan, et al. (CMS), Observation of charge-dependent azimuthal correlations in p -Pb collisions and its implication for the search for the chiral magnetic effect, *Phys. Rev. Lett.* 118 (2017) 122301. doi:doi:10.1103/PhysRevLett.118.122301. [arXiv:1610.00263](#).
- [24] A. M. Sirunyan, et al. (CMS), Constraints on the chiral magnetic effect using charge-dependent azimuthal correlations in p Pb and PbPb collisions at the CERN Large Hadron Collider, *Phys. Rev. C* 97 (2018) 044912. doi:doi:10.1103/PhysRevC.97.044912. [arXiv:1708.01602](#).
- [25] S. Acharya, et al. (ALICE), Constraining the magnitude of the Chiral Magnetic Effect with Event Shape Engineering in Pb-Pb collisions at $\sqrt{s_{NN}} = 2.76$ TeV, *Phys. Lett. B* 777 (2018) 151–162. doi:doi:10.1016/j.physletb.2017.12.021. [arXiv:1709.04723](#).
- [26] M. I. Abdulhamid, et al. (STAR), Estimate of background baseline and upper limit on the chiral magnetic effect in isobar collisions at $s_{NN}=200$ GeV at the BNL Relativistic Heavy Ion Collider, *Phys. Rev. C* 110 (2024) 014905. doi:doi:10.1103/PhysRevC.110.014905. [arXiv:2310.13096](#).
- [27] J. Chen, et al., Properties of the QCD Matter – An Experimental Review of Selected Results from RHIC BES Program (2024). [arXiv:2407.02935](#).
- [28] D. E. Kharzeev, J. Liao, P. Tribedy, Chiral Magnetic Effect in Heavy Ion Collisions: The Present and Future (2024). [arXiv:2405.05427](#).
- [29] J. Liao, V. Koch, A. Bzdak, On the Charge Separation Effect in Relativistic Heavy Ion Collisions, *Phys. Rev. C* 82 (2010) 054902. doi:doi:10.1103/PhysRevC.82.054902. [arXiv:1005.5380](#).
- [30] S. Pratt, S. Schlichting, S. Gavin, Effects of Momentum Conservation and Flow on Angular Correlations at RHIC, *Phys. Rev. C* 84 (2011) 024909. doi:doi:10.1103/PhysRevC.84.024909. [arXiv:1011.6053](#).
- [31] F. Wang, J. Zhao, Challenges in flow background removal in search for the chiral magnetic effect, *Phys. Rev. C* 95 (2017) 051901. doi:doi:10.1103/PhysRevC.95.051901. [arXiv:1608.06610](#).
- [32] Y. Feng, J. Zhao, F. Wang, Responses of the chiral-magnetic-effect-sensitive sine observable to resonance backgrounds in heavy-ion collisions, *Phys. Rev. C* 98 (2018) 034904. doi:doi:10.1103/PhysRevC.98.034904. [arXiv:1803.02860](#).
- [33] W.-Y. Wu, et al., Global constraint on the magnitude of anomalous chiral effects in heavy-ion collisions, *Phys. Rev. C* 107 (2023) L031902. doi:doi:10.1103/PhysRevC.107.L031902. [arXiv:2211.15446](#).
- [34] Z. Xu, B. Chan, G. Wang, A. Tang, H. Z. Huang, Event shape selection method in search of the chiral magnetic effect in heavy-ion collisions, *Phys. Lett. B* 848 (2024) 138367. doi:doi:10.1016/j.physletb.2023.138367. [arXiv:2307.14997](#).
- [35] D. Shen, J. Chen, A. Tang, G. Wang, Impact of globally spin-aligned vector mesons on the search for the chiral magnetic effect in heavy-ion collisions, *Phys. Lett. B* 839 (2023) 137777. doi:doi:10.1016/j.physletb.2023.137777. [arXiv:2212.03056](#).
- [36] Z.-T. Liang, X.-N. Wang, Globally polarized quark-gluon plasma in non-central A+A collisions, *Phys. Rev. Lett.* 94 (2005) 102301. doi:doi:10.1103/PhysRevLett.94.102301.
- [37] Z.-T. Liang, X.-N. Wang, Spin alignment of vector mesons in non-central A+A collisions, *Phys. Lett. B* 629 (2005) 20–26. doi:doi:10.1016/j.physletb.2005.09.060. [arXiv:nucl-th/0411101](#).
- [38] B. I. Abelev, et al. (STAR), Spin alignment measurements of the $K^*(892)$ and $\phi(1020)$ vector mesons in heavy ion collisions at $\sqrt{s_{NN}}=200$ GeV, *Phys. Rev. C* 77 (2008) 061902. doi:doi:10.1103/PhysRevC.77.061902. [arXiv:0801.1729](#).
- [39] S. Acharya, et al. (ALICE), Evidence of Spin-Orbital Angular Momentum Interactions in Relativistic Heavy-Ion Collisions, *Phys. Rev. Lett.* 125 (2020) 012301. doi:doi:10.1103/PhysRevLett.125.012301. [arXiv:1910.14408](#).
- [40] M. S. Abdallah, et al. (STAR), Pattern of global spin alignment of ϕ and K^* mesons in heavy-ion collisions, *Nature* 614 (2023) 244–248. doi:doi:10.1038/s41586-022-05557-5. [arXiv:2204.02302](#).
- [41] S. Acharya, et al. (ALICE), Measurement of the J/ψ Polarization with Respect to the Event Plane in Pb-Pb Collisions at the LHC, *Phys. Rev. Lett.* 131 (2023) 042303. doi:doi:10.1103/PhysRevLett.131.042303. [arXiv:2204.10171](#).

- [42] L. Adamczyk, et al. (STAR), Global Λ hyperon polarization in nuclear collisions: evidence for the most vortical fluid, *Nature* 548 (2017) 62–65. doi:doi:10.1038/nature23004. [arXiv:1701.06657](#).
- [43] J. Adam, et al. (STAR), Global polarization of Λ hyperons in Au+Au collisions at $\sqrt{s_{NN}} = 200$ GeV, *Phys. Rev. C* 98 (2018) 014910. doi:doi:10.1103/PhysRevC.98.014910. [arXiv:1805.04400](#).
- [44] S. Acharya, et al. (ALICE), Global polarization of $\Lambda\bar{\Lambda}$ hyperons in Pb-Pb collisions at $\sqrt{s_{NN}} = 2.76$ and 5.02 TeV, *Phys. Rev. C* 101 (2020) 044611. doi:doi:10.1103/PhysRevC.101.044611. [arXiv:1909.01281](#).
- [45] M. S. Abdallah, et al. (STAR), Global Λ -hyperon polarization in Au+Au collisions at $\sqrt{s_{NN}}=3$ GeV, *Phys. Rev. C* 104 (2021) L061901. doi:doi:10.1103/PhysRevC.104.L061901. [arXiv:2108.00044](#).
- [46] Y.-G. Yang, R.-H. Fang, Q. Wang, X.-N. Wang, Quark coalescence model for polarized vector mesons and baryons, *Phys. Rev. C* 97 (2018) 034917. doi:doi:10.1103/PhysRevC.97.034917. [arXiv:1711.06008](#).
- [47] X.-L. Sheng, L. Oliva, Q. Wang, What can we learn from the global spin alignment of ϕ mesons in heavy-ion collisions?, *Phys. Rev. D* 101 (2020) 096005. doi:doi:10.1103/PhysRevD.101.096005. [arXiv:1910.13684](#).
- [48] X.-L. Xia, H. Li, X.-G. Huang, H. Zhong Huang, Local spin alignment of vector mesons in relativistic heavy-ion collisions, *Phys. Lett. B* 817 (2021) 136325. doi:doi:10.1016/j.physletb.2021.136325. [arXiv:2010.01474](#).
- [49] J.-H. Gao, Helicity polarization in relativistic heavy ion collisions, *Phys. Rev. D* 104 (2021) 076016. doi:doi:10.1103/PhysRevD.104.076016. [arXiv:2105.08293](#).
- [50] X.-L. Sheng, Q. Wang, X.-N. Wang, Improved quark coalescence model for spin alignment and polarization of hadrons, *Phys. Rev. D* 102 (2020) 056013. doi:doi:10.1103/PhysRevD.102.056013. [arXiv:2007.05106](#).
- [51] X.-L. Sheng, L. Oliva, Z.-T. Liang, Q. Wang, X.-N. Wang, Spin alignment of vector mesons in heavy-ion collisions, *Phys. Rev. Lett.* 131 (2023) 042304. doi:doi:10.1103/PhysRevLett.131.042304.
- [52] J. Chen, Z.-T. Liang, Y.-G. Ma, Q. Wang, Global spin alignment of vector mesons and strong force fields in heavy-ion collisions, *Sci. Bull.* 68 (2023) 874–877. doi:doi:10.1016/j.scib.2023.04.001. [arXiv:2305.09114](#).
- [53] X.-L. Sheng, L. Oliva, Z.-T. Liang, Q. Wang, X.-N. Wang, Relativistic spin dynamics for vector mesons, *Phys. Rev. D* 109 (2024) 036004. doi:doi:10.1103/PhysRevD.109.036004.
- [54] J.-H. Chen, Z.-T. Liang, Y.-G. Ma, X.-L. Sheng, Q. Wang, Vector meson's spin alignments in high energy reactions (2024). [arXiv:2407.06480](#).
- [55] B. Müller, D.-L. Yang, Anomalous spin polarization from turbulent color fields, *Phys. Rev. D* 105 (2022) L011901. doi:doi:10.1103/PhysRevD.105.L011901. [arXiv:2110.15630](#).
- [56] J.-p. Lv, Z.-h. Yu, Z.-t. Liang, Q. Wang, X.-N. Wang, Global quark spin correlations in relativistic heavy ion collisions, *Phys. Rev. D* 109 (2024) 114003. doi:doi:10.1103/PhysRevD.109.114003. [arXiv:2402.13721](#).
- [57] K. Ackerstaff, et al. (OPAL), Spin alignment of leading $K^*(892)0$ mesons in hadronic $Z0$ decays, *Phys. Lett. B* 412 (1997) 210–224. doi:doi:10.1016/S0370-2693(97)01077-0. [arXiv:hep-ex/9708022](#).
- [58] Z.-W. Lin, C. M. Ko, B.-A. Li, B. Zhang, S. Pal, A Multi-phase transport model for relativistic heavy ion collisions, *Phys. Rev. C* 72 (2005) 064901. doi:doi:10.1103/PhysRevC.72.064901. [arXiv:nucl-th/0411110](#).
- [59] S. Lan, Z.-W. Lin, S. Shi, X. Sun, Effects of finite coverage on global polarization observables in heavy ion collisions, *Phys. Lett. B* 780 (2018) 319–324. doi:doi:10.1016/j.physletb.2018.02.076. [arXiv:1710.03895](#).
- [60] D. Shen, J. Chen, Z.-W. Lin, The effect of hadronic scatterings on the measurement of vector meson spin alignments in heavy-ion collisions, *Chin. Phys. C* 45 (2021) 054002. doi:doi:10.1088/1674-1137/abe763. [arXiv:2102.05266](#).
- [61] D. Shen, J. Chen, A. Tang, G. Wang, Influence of globally spin-aligned vector mesons to the measurements of the chiral magnetic effect in heavy-ion collisions, *EPJ Web Conf.* 296 (2024) 04002. doi:doi:10.1051/epjconf/202429604002.